

Experimental Assessment of Fatigue and Tensile Strength on Ageing Properties of Al-Zn-Mg Alloys

P. K. Mandal

Department of Metallurgical & Materials Engineering, Indian Institute of Technology Roorkee, Roorkee, Pin-247667, India.

Article history

Received: 05-June-2015

Revised: 28-Aug-2015

Available online: 04-Sep-2015

Keywords:

Fatigue strength,
Ageing,
SEM,
Al-Zn-Mg-Sc alloy

Abstract

The high strength Al-Zn-Mg alloy was widely used in aerospace engineering due to generosity of age-hardening properties. The fatigue strength and tensile properties on age-hardening response were measured for a common Al-Zn-Mg and Al-Zn-Mg-Sc alloys. When Sc inoculation has been accelerated ageing properties in Al-Zn-Mg alloy. Inhomogeneity in microstructure and mechanical performances of coarse particle influence the fatigue crack initiation life. The fatigue test parameters were selected such as amplitude 2-4 KN, f = 2 Hz with variable R ratios. The optimum fatigue crack resistance was evaluated from S-N curves of $\approx 2 \times 10^6$ cycles for cast Al-Zn-Mg-Sc alloy at T_6 condition. The tensile properties were optimized at T_6 condition of 0.2% PS 355.0 MPa, UTS 446.6 MPa and ductility 4.2% for cast Al-Zn-Mg-Sc alloy. Experimental characterizations have done through microstructural evaluation, Vicker's hardness measurement of age-hardening effects, mechanical testing, SEM analysis on fracture surfaces, FESEM and TEM analysis.

*The work had been presented at an international conference **Fatigue Durability India 2015**, 28-30th May 2015, JN TATA AUDITORIUM, Indian Institute of Science, Bangalore.*

© 2015 JMSSE All rights reserved

Introduction

The optimum tensile strength and fatigue life are the two major criterions for high strength Al-Zn-Mg alloy. It is also well-established that fatigue life of components is strongly influenced by the fine grains and ageing treatment [1, 2]. If the cast Al-Zn-Mg alloy can be modified against crack initiation, fatigue life improvement can also be expected. Moreover, inhomogeneity in microstructure and mechanical performances of ageing precipitation of cast Al-Zn-Mg alloys influences the fatigue crack initiation life. Main emphasis has been employed on understanding the mechanical driving forces and materials ageing response for fatigue crack formation and growth in high strength as-cast aluminium alloys. However, several studies have been shown that fatigue crack initiation life is about 40 – 50% of the total life for endurances from 10^5 to 10^6 cycles. It is also major benefit to fatigue design for engineering components to be accurately predicted mechanism of fatigue crack initiation such as cast aluminium alloys [3-5]. Therefore, grain refinement by Sc (scandium) inoculation for fatigue life improvement is the advanced topic which is ultimately discussed. For aluminium alloy, size and shape of the grains can be important in determining the performance in structural applications [6-8]. Fine grain size is beneficial to aluminium alloy for ambient temperature structural use, because it simultaneously gives high strength and better fatigue crack resistance. Specially, grain refinement can decrease the size of defects and eliminate hot tearing for large and high strength aluminium alloy ingots. Many researchers had been quoted on grain refinement achieve by heterogeneous nucleation the use of inoculants and by alloying elements [Rosenhain, 1930; Cibula, 1951-1952; Murthy, 2002]. Generally, grain size is inversely related to the degree of undercooling due to an increased nucleation rate [9]. There are many principle effects that can be obtained by the adding Sc to Al-Zn-Mg alloys likely to grain

refinement, precipitation hardening from ScAl_3 particles and grain structure control from ScAl_3 dispersoids [10]. Therefore, a small amount of Sc (lightest transition metal) to aluminium alloy causes drastic hardening by the homogenous of fine $\text{L1}_2\text{-ScAl}_3$ particles from a supersaturated solid solution, while grain refinement is achieved by the ScAl_3 phase. On the other hand, the ageing treatment relies on the fine precipitation from the supersaturated solid solution (SSSS) which is associated with nucleation and growth process. The main precipitates are the $\text{Al}_2\text{Mg}_3\text{Zn}_3$ and MgZn_2 phases with ScAl_3 form in α -Al matrix [11-16]. Coarse particles and phases present in these cast alloys were identified by FESEM with EDS and TEM with EDX analysis. Finally, SEM observations were performed for the three types of cast aluminium alloy of crack propagation paths illustrating the typical microstructures. In this paper, several experimental characterizations have carried out through microstructural evaluation, Vicker's hardness measurement of age-hardening effects, tensile testing, fatigue testing, SEM analysis of tensile and fatigue fracture surfaces, FESEM and TEM analysis.

Experimental

The three types of Al-Zn-Mg alloy was cast using pure Zn and pure Mg with Sc (in form of Al-2 wt.% master alloy) grain refiner. The initial size of cast plate was $160 \times 90 \times 24$ mm³. For the alloy production the Al melt was heated up to 780 ± 5 °C with total time taken of 3 h and the Al-Sc master alloy addition was incorporated to carefully handle Sc fading effect during melting. The composition of the alloy was examined by ICP-AES (inductively coupled plasma atomic emission spectroscopy) and the following chemical composition has shown in Table-1. The alloy was subjected to optical microscopic analysis using LEICA DMI 5000M (Leica Microsystems, Buffalo Grove, IL) microscope after thoroughly metallographic polishing and etching by modified

Keller's reagent (2.5 ml HNO₃ (70%)+1.5 ml HCl (38%)+1 ml HF(40%)+ 175 ml water) as shown in Fig.-1. The FESEM micrographs with EDS analysis were carried out on as-cast samples (QUANTA 200F, FEG LaB₆, 30kV) as shown in Fig.-2. The as-cast alloy was subjected to solution treatment at 465±5 °C for 1h followed by water quenching and kept for one week in room temperature for natural ageing and then prefers artificial ageing at 120±2 °C, 140±2 °C and 180±2 °C for 16h in air atmosphere, respectively. In each time, Vicker's hardness (Model no.: FIE-VM50 PC) measurements were performed on T₄ alloy (solution treated + water quenching and room temperature ageing) at 10 kg. load with 15 sec dwell time. The Vicker's hardness measurements on ageing kinetics have been shown in graphical representation in Fig.-3 for three ageing temperatures upto 16h ageing time. The Vicker's hardness values were selected of average six indentations of each time in hardness measurement. TEM analysis with EDX has been carried out to study the precipitation morphology, composition, size, and orientation using at Techai G² 20 S-TWIN at 200 kV as shown in Fig.-4. Consequently, the fracture surface of tensile and fatigue specimens have studied by scanning electron microscopy (SEM) (Model no.: LEO 435 VP) analysis as shown in Fig.-5 and Fig.-6, respectively. The fatigue tests were performed using a fatigue testing machine (Instron Model no. 1342) at a variable stress ratio of R<1 with tension-tension cyclic loading types. Different stress amplitudes (2 KN, 4 KN) were loaded in the sinusoidal wave form at a frequency about 2 Hz. All fatigue tests were conducted in air at room temperature and results shown in Fig.-7. The fatigue specimen dimensions are 100 mm full length, 40 mm gauge length, 6.4 mm thickness as shown in Fig.-8. The tensile test specimens were cut from cast plate (150 × 90 × 24 mm³) of studied alloys. Consequently, the tensile test was performed at room temperature using Instron (universal testing machine) UTM (25 KN, H25 K-S, UK). All specimen dimensions were 5 mm gauge diameter and 25 mm gauge length and tested with cross head speed 1 mm/min. The results of the tensile test are illustrated in bar diagrams as shown in Fig.-9.

Table 1: Chemical composition analyzed by ICP-AES method of studied aluminium alloys (7xxx series) in wt. %.

Alloy nos.	Zn	Mg	Sc	Si	Fe	Al	Zn + Mg
1	5.76	2.57	-	0.10	0.10	Bal.	8.33
2	9.75	3.80	-	0.10	0.22	Bal.	13.55
3	6.47	1.54	0.33	0.19	0.21	Bal.	8.01

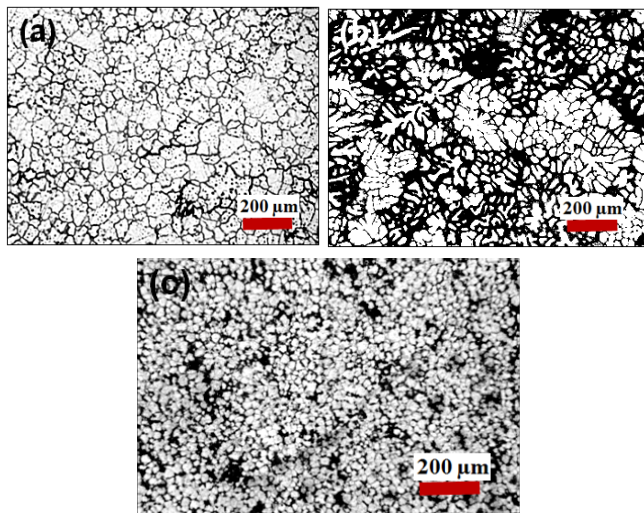


Figure 1: Illustration of optical micrograph of studied alloys (as-cast condition): (a) Alloy-1, (b) Alloy-2, (c) Alloy-3.

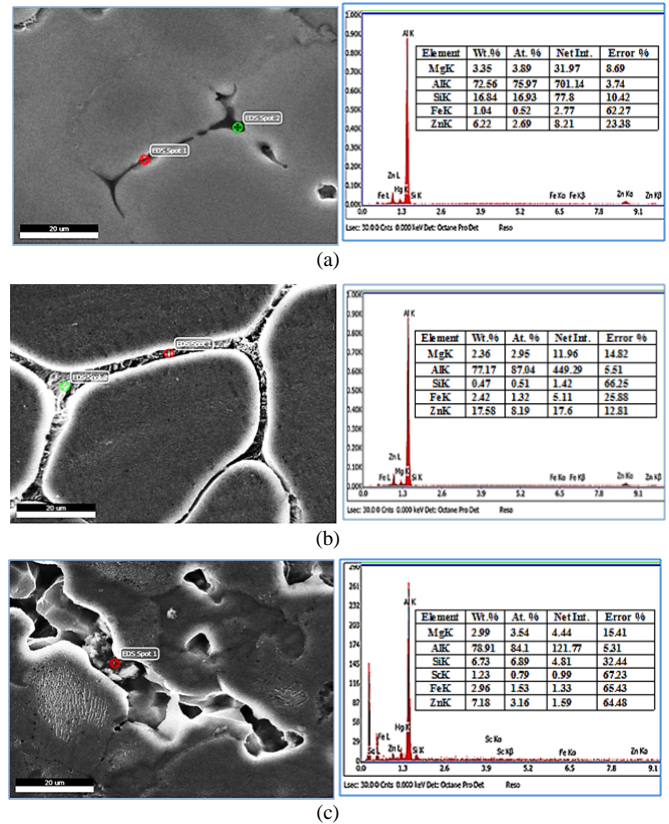


Figure 2: FESEM micrographs with EDS analysis of as-cast alloys: (a) Alloy-1, (b) Alloy-2, (c) Alloy-3.

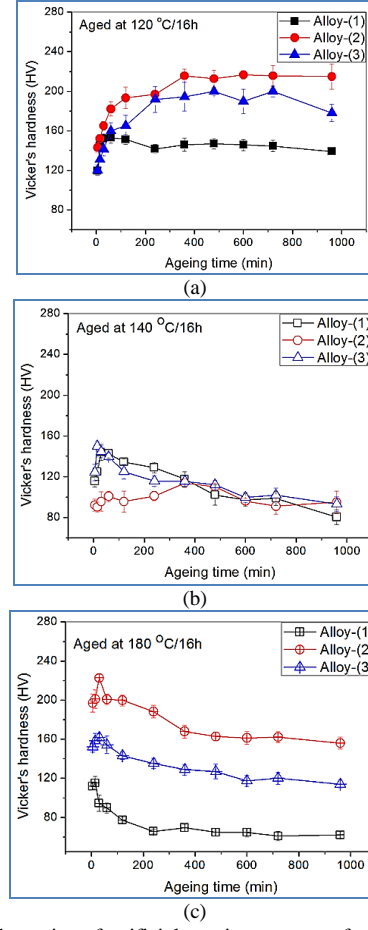


Figure 3: Illustration of artificial ageing curve of studied alloys at different temperatures: (a) at 120 °C, (b) at 140 °C, (c) at 180 °C.

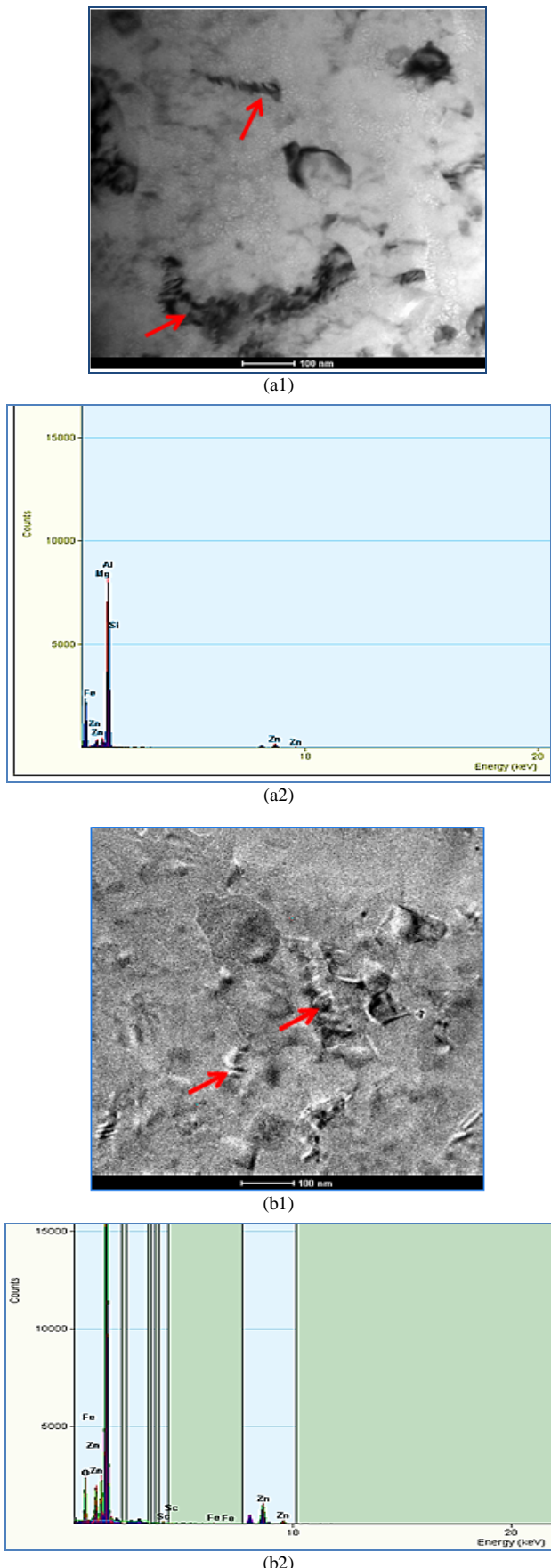


Figure 4: TEM micrograph with EDX analysis of as-cast alloys: (a) Alloy-1, (b) Alloy-3.

Results and Discussion

An experimental assessment of the precipitation processes in high strength Al-Zn-Mg alloy has been presented due to its attractive mechanical properties [17]. Artificial ageing characterization was evaluated through Vicker's hardness measurement for these alloys, based upon 7xxx series with duplex treatments (i.e., natural ageing and artificial ageing) widely used in industries [18]. It is also mentioned that after Sc inoculated in Al-Zn-Mg alloy refine grains as well as accelerated ageing kinetics. In this experimental study, one solution temperature (at 465 °C) has been considered and the response to several artificial ageing treatments analyzed in the range of 120 to 180 °C. This heat treatment is performed over a wide range of temperatures, usually several steps. The first step ranges from 100 to 120 °C which is within the stability range of GP zones, and the second step from 140 to 170 °C which is the temperature range for η and η precipitation and so on [19, 20]. In summary, Zn and Mg as the major alloying elements in Al-Zn-Mg alloy system play an important role in the formation of the precipitated phases in the alloy, especially for η ($MgZn_2$) phase, and $T(Al_2Mg_3Zn_3)$ phase based on the assumption that the varied elements acts alone without interactions with other alloying elements [21, 22]. Moreover, Sc elements in Al-Zn-Mg alloy mainly exist as $ScAl_3$ particles. Primary $ScAl_3$ particles can refine the casting structures, which leads to fine grain. Secondary $ScAl_3$ particles can produce substructure strengthening and precipitation strengthening. So, present studied alloys in a supersaturated solid solution after casting, Sc elements precipitate into fine coherent $ScAl_3$ particles during subsequent heat treatment and contribute to increased strength. In addition, the most important strengthening mechanisms of Sc in aged Al-Zn-Mg alloys were Orowan strengthening of secondary $ScAl_3$ particles [23, 6]. The optical micrograph of the studied alloys is shown in Fig.-1. Coarsened as-cast grains, dendritic structures, segregation and eutectic formation on grain boundary observed in the Alloy-1 and Alloy-2 [Fig.-1(a-b)]. While, minor Sc can significantly refine the as-cast grain in the Alloy-3. In the Alloy-3 minor Sc (0.33%) addition dendritic structure completely disappeared to obtain fine average grains size of 22 μm [Fig.-1(c)]. Similarly, as-cast grain size measured to Alloy-1 and Alloy-2 as 50.3 μm and 33.5 μm , respectively. The FESEM micrographs with EDS analysis revealed grain boundary segregation for Zn, Mg solute elements with Sc surplus of $ScAl_3$ agglomeration have been examined of as-cast alloys in Fig.-2(a-c). It showed that high solute content (13.55 wt.%) detection has found out of Alloy -2 [Fig.-2 (b)]. It showed that primary $ScAl_3$ phases are present due to nonequilibrium concentration during solidification of Alloy-3 [Fig.-2(c)]. In Fig.-3(a-c) exhibited of artificial ageing curves through Vicker's hardness measurement of studied alloys after T_4 heat treatment and so on. In Fig.-3(a) shows at 120 °C ageing phenomena of studied alloys when highest hardening effect due to GP zones formation with high density of solute atoms of Alloy-2. It is also beneficial effects of high solute content to maintain high hardness throughout in this age hardening regime. In Fig.- 3(b) shows at 140 °C ageing phenomena of studied alloys when usual hardening effect due to moderate solute contents to formation of GP-II zones (form above 120 °C) and may transform to semi-coherent η phases of Alloy-1. But overall less hardening effects have been shown in 140 °C ageing regime because incoherency derive very faster rate for cast aluminium alloys. Moreover, main hardening phase η with $ScAl_3$ particles (for Sc added alloy) incoherency dominated overaged condition. In Fig.-3(c) shows at 180 °C ageing phenomena of studied alloys when highest hardening effect due to high solute contents to formation of η phases transformation for Alloy-2. At this high temperature maintain continuous ageing properties due to high solutes content to formation of η phases and $ScAl_3$ particles coherency (for Sc added

alloy). But all three ageing temperatures exhibited early ageing peaks (within 1 to 2h) as ageing temperature increases fact of GP zones formation with Sc inoculation (for Sc added alloy) to accelerate of ageing kinetics at faster rate. In Fig.-4(a-b) shows TEM micrograph with EDX analysis on as-cast alloys. When EDX analysis conformed Zn and Mg solutes with Sc existence of as-cast alloys. In Fig-4(a) exhibited grain boundary segregation of solute atoms as shown in red arrows of as-cast Alloy-1. In Fig-4(b) exhibited mainly cuboid of ScAl_3 particles with cauliflower shape as shown in red arrows of as-cast Alloy-3. The aluminium alloys usually show a ductile fracture with microvoids coalescence mechanism, in these alloys the examined fracture surfaces exhibited a predominately brittle fracture. Remained second phase constituents, narrow-weak precipitation free zone (PFZ) and coarser precipitates that are grain boundary characteristics of age-hardenable 7xxx series aluminium alloys tend to favour intergranular fracture by stress concentration in conjunction site of the grains and so crack initiation and propagation along high angle grain boundaries. In Fig.-5(a-c) shows the fractured surface at low and high magnification of tensile specimens at as-cast condition under SEM analysis. As it is seen, all the studied alloys shows cast inhomogeneity which indicating that the fracture occurs in a brittle mode. Coarse intermetallics at grain boundaries cause initiation of cracks and fast intergranular crack propagation. For Alloy-1 [in Fig.-5(a)] as-cast grains revealed which mostly intergranular fracture initiated at the grain boundary regions that the prominent at low magnification fracture surface as indicated by red arrows. For Alloy-2 [in Fig.-5(b)] as-cast grains revealed with coarse second phases due to high solute contents (13.55 wt.%) as indicated by red arrows that the initiation of secondary crack inside grains. For Alloy-3 [in Fig.-5(c)] as-cast equiaxed grains revealed due to grain refinement of Sc inoculation but cracks initiated along the grains boundary also volume of cracks more in this case. So, interlink of among the cracks accelerated fracture propagation during tensile stress.

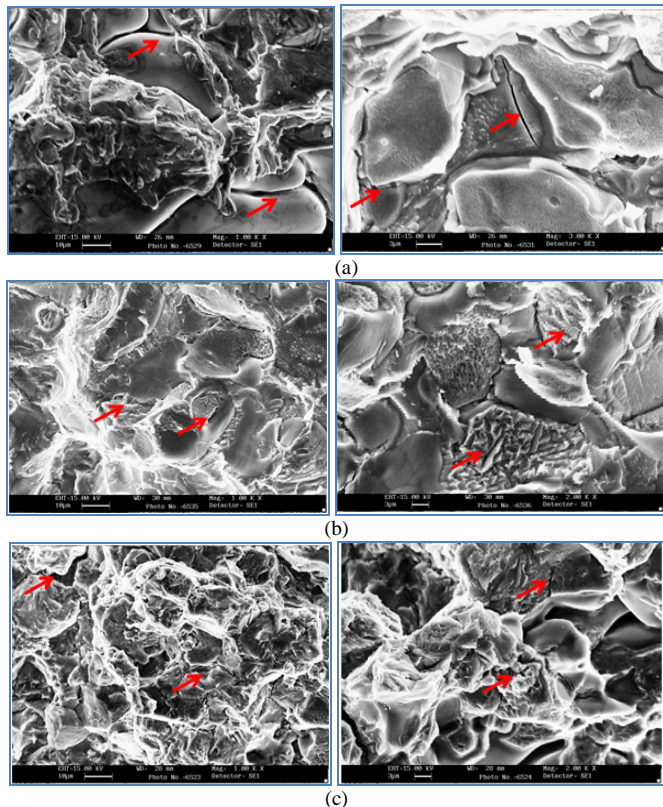


Figure 5: The illustration of SEM tensile fracture surface of as-cast alloys at different conditions (at low and high magnifications): (a) Alloy-1, (b) Alloy-2, (c) Alloy-3.

All fatigue fracture surfaces are examined by SEM analysis. In Fig.-6(a) show the fatigue striation which follow continuously across a secondary crack (for high magnification fractograph). The secondary cracking in the flat fracture category specimen along the grain boundaries is a puzzling feature since this crack propagate parallel to the tensile axis [24]. In Fig.-6(b) show the fatigue fracture morphologies of the Alloy-2 in the as-cast condition has characterized by ductile transgranular rupture, with a component of intergranular fracture and secondary cracking. It is also found that the micocracks initiated around the coarse second phases, $\text{T}(\text{Al}_2\text{Zn}_3\text{Mg}_3)$ as shown in red arrows. While the small dimples is associated with the smaller, more fine, dispersoids as shown in high magnification fracture surface. But for low magnification fracture surface exhibited transgranular microcracks generated around the coarse second phase as well as sharp continuous crack line networks revelation in matrix. In Fig.-6(c) show the fatigue fracture morphologies of the Alloy-3 in the as-cast condition has characterized by ductile intergranular rupture followed by equiaxed grains with continuous cracking networks throughout of matrix in both the magnifications. Also, spotted several dip holes those might be stress concentration points or stress raiser points. At low magnification disclosed several microholes those might be porosity or cast inhomogeneities of such as-cast alloy. Grain refinement caused by Sc inoculation contributed individual grain to fatigue cracks resistance as a result high number of cycles to failure under constant maximum applied stress at T_6 condition (aged at 160 °C for 2h).

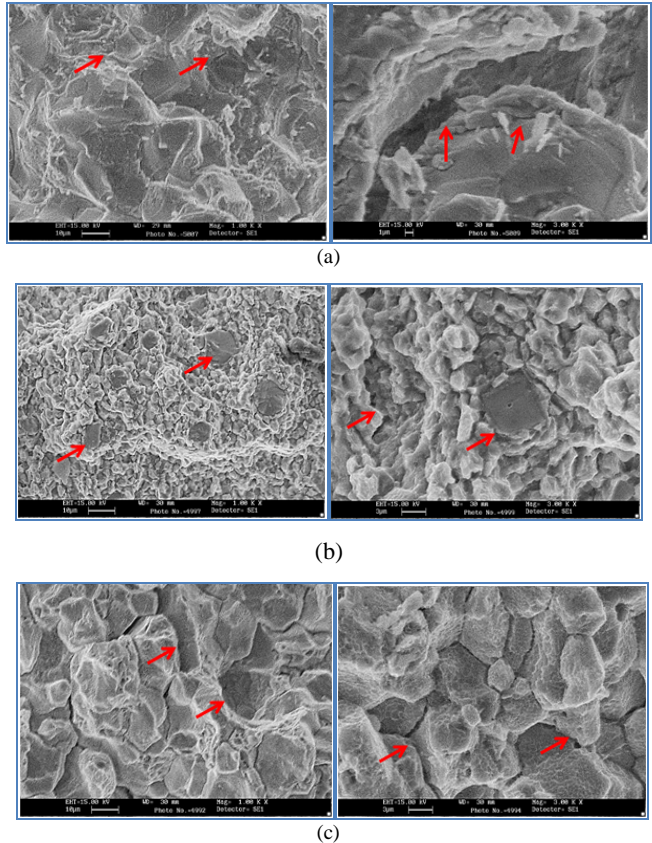


Figure 6: The illustration of SEM fatigue fracture surfaces at different conditions (at low and high magnifications): (a) Alloy-1(at as-cast condition), (b) Alloy-2 (at as-cast condition), (c) Alloy-3 (at T_6 condition).

Fatigue is the phenomenon of mechanical property degradation to failure of a component under cyclic loading. The main approach of fatigue testing is stress vs number of cycles, S-N curve. In this conventional approach defect free specimen is subjected to cyclic

loading at known stress value and the number of cycles at which specimen fails to recorded. The stress value vs number of cycles the specimens withstand during cyclic loading is plotted to get S-N curve as shown in Fig.-7. The significant drawback of such studies is that no distinction can be made between the crack initiation stage and the crack propagation stage. However, cast specimens generally show lower fatigue strength due to porosity, inclusion, segregation and other casting defects. Thus, the high strength of studied alloy was mainly associated with the fine grain strengthening caused by the addition of Sc and the subgrain strengthening of ScAl_3 particles and η precipitates. Since, Al-Zn-Mg alloy is age-hardening ability to precipitates out fine coherent GP zones with η -phases to strengthen the matrix. In Fig.-7 shows of Alloy-1(for black circle notation) very low fatigue strength at this following parameters because cast inhomogeneity, porosity and slag entrapment main cause of failure for low fatigue cycles. Consequently, for Alloy-2 (for red square notation) shows moderate fatigue strength due to high solute content main cause of high fatigue cycles to formation of more numbers of GP zones and η phases during testing. For Alloy-3 (for black square notation) shows low and high fatigue strength due to cast inhomogeneity, porosity and slag entrapment main cause of failure for low fatigue cycles (<50000 cycles) but for high fatigue strength due to fine grains with ScAl_3 particles coherency (misfit only 1.5%) with α -Al matrix. Moreover, from all effects of Sc addition plus T_6 heat treatment as above mentioned, fatigue lifetime improvement should be expected. From this diagram in Fig.-7 shows the beneficial effect of a Sc inoculation with T_6 heat treatment of Al-Zn-Mg-Sc alloy on fatigue lifetime enhancement are seen particularly for in the high cycle fatigue (HCF) regime (≤ 200000 cycles).

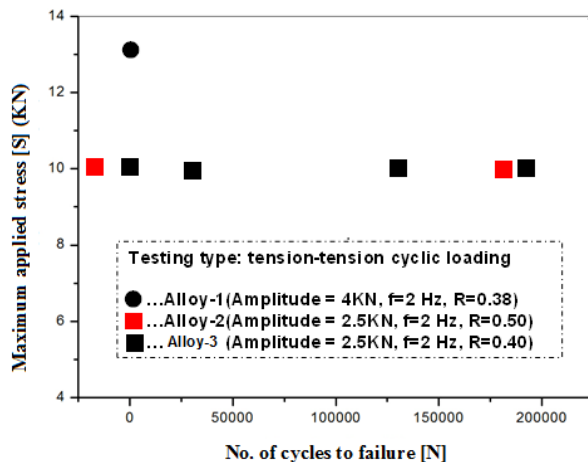


Figure 7: S-N plots for different aluminium alloys.

The tensile properties of the studied aluminium alloys mainly depend on the shape, size and the size distribution of the α -Al grains, eutectic structure and the distribution of the intermetallics in the interdendritic region. The main reason for this improvement is high probability due to the reduced grain size of the castings, leading to a finer distribution of second phases (i.e., MgZn_2 , ScAl_3 etc.). It is well known that according to Hall-Patch theory the finer the grains, the higher the strength. So the small and dispersed ScAl_3 particles will provide a large force to retard the movement of dislocations and enhance the strength of Alloy-3. The addition of 0.33 wt.% Sc has led to improved tensile properties by reducing the volume fraction of eutectic phases, as well as by fining the grain size. It is seen that [in Fig.-9], all studied alloys tensile properties enhanced after T_6 heat treatment. But for Alloy-3 tensile properties enhanced remarkably at T_6 condition, i.e., 0.2% proof stress (PS) rises from 288.0 MPa to 355 MPa, UTS (ultimate

tensile stress) rises from 294.2 MPa to 446.6 MPa, ductility improve 4.0 % to 4.2%. Therefore, several reports indicated that metastable coherent or semicoherent η precipitates and ScAl_3 are formed during ageing treatment.

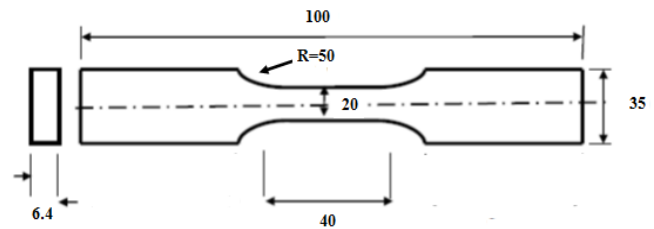


Figure 8: Schematic diagram of the tensile fatigue specimen (all dimensions in mm).

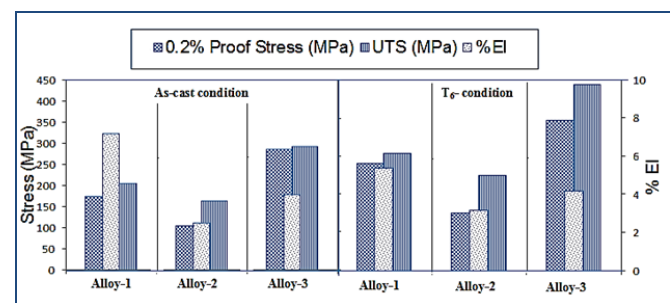


Figure 9: The bar diagram exhibited of tensile properties of studied alloys at as-cast and T_6 (aged 160 °C/2h) conditions.

Conclusions

1. The addition of 0.33 wt.% Sc to a 7xxx alloy has resulted a finer grain structure leading to improve tensile and fatigue strength properties.
2. The aluminium alloys were artificially aged to T_6 condition. They were first solution treated at 465 °C for 1h and subsequently water quenched and followed by ageing 160 °C for 2h. Then alloys evaluated different mechanical properties such as tensile strength and fatigue properties.
3. The addition of Sc improves the mechanical properties of the as-cast Al-Zn-Mg alloy. The reason is the precipitation of secondary ScAl_3 particles and the remarkable refinement of the grains, such as precipitation strengthening and fine grains strengthening.
4. Fine grains achieved through Sc inoculation in Al-Zn-Mg alloy which serve to inhibit or retard crack initiation as well as fatigue crack growth. Consequently, the fatigue lifetime can be improved considerably through Sc inoculation with ageing effects (i.e., T_6 treatment) in high strength as-cast Al-Zn-Mg-Sc alloy.
5. Grain refinement by the addition of Sc (0.33 wt.%) in Aluminium alloy and T_6 heat treatment improves tensile strength and fatigue fracture limit. SEM analysis of fracture surface of the specimens revealed an intergranular fracture in as-cast alloys, whereas cracking of individual second phases was responsible for fracture behaviour of studied alloys.
6. Fatigue strength depends on strength/hardness. The hardness increases with Sc addition with T_6 heat treatment or age-hardening treatment, so enhanced the fatigue strength (number of cycles to failure at a given stress).
7. After heat treatment (T_6), the Alloy-3 have shown the following optimum mechanical properties: $\sigma_{0.2}$ (0.2% proof stress) = 355.0 MPa, σ_u (UTS) = 446.6 MPa, δ (ductility) =

4.2% and fatigue fracture limit in terms of number of cycles to failure (HCF) = ≤ 200000 as shown in S-N plot.

Acknowledgements: The author is grateful for financial support to carry out experimental works to provide MHRD fellowship from Department of Metallurgical & Materials Engineering in IIT Roorkee.

References

1. Chen, Z., Mo, Y., Nie, Z.: Effect of Zn Content on the Microstructure and Properties of Super-High Strength Al-Zn-Mg-Cu Alloys, *Metallurgical and Materials Transactions A*, Vol. 44A, August 2013, pp. 3910-3920.
2. Chemingui, M., Khitouni, M., Jozwiak, K., Mesmacque, G., Kolsi, A.: Characterization of the mechanical properties changes in an Al-Zn-Mg alloy after a two-step ageing treatment at 70° and 135 °C, *Materials and Design*, 31 (2010) pp. 3134-3139.
3. Zhang, L., Liu, X., Wang, L., Wang, P.: Fatigue crack initiation for Al-Zn-Mg alloy welded joint, *Acta Metallurgica Sinica*, Vol. 25, No. 3, June 2012, pp. 235-240.
4. Nikitin, S.L., Men II, D.: Al-Zn-Mg-Based Cast Alloys Having Mechanical Properties, *Russian Metallurgy (Metally)*, Vol. 2010, No. 1, pp. 41-47.
5. Huang, J-w., Yin, Z-m., Fang, J-f., Nie, B., Wang, T.: Aging Characteristics of 7A52 Al-Zn-Mg Alloy, *Materials Science Forum*, Vols. 546-549, 2007, pp. 867-870.
6. Dai, X-y., Xia, C-q., Wu, A-r., Peng, X-m.: Influence of Scandium on Microstructures and Mechanical Properties of Al-Zn-Mg-Cu-Zr Alloys, *Materials Science Forum*, Vols. 546-549 (2007), pp. 961-964.
7. DuQuesnay, D.L., Underhill, P.R., Britt, H.J., Fatigue crack growth from corrosion damage in 7075-T6511 aluminium alloy under aircraft loading, *International Journal of Fatigue*, 25, 2003, pp. 371-377.
8. Dumont, D., A. Deschamps, Brechet, Y.: A model for predicting fracture mode and toughness in 7000 series aluminium alloys, *Acta Materialia*, 52, 2004, pp. 2529-2540.
9. Murty, B.S., Kori, S.A., Chakraborty, M.: Grain refinement of aluminium and its alloys by heterogeneous nucleation and alloying, *International Materials Reviews*, Vol. 47, No. 1, 2002, pp. 3-29.
10. Ahmed, Z.: The Properties and Application of Scandium-Reinforced Aluminium, *Journal of Minerals, Metals and Materials Society*, Vol. 55, Issue 2, February 2003, pp. 35-39.
11. Mandal, P.K., Ghosh, P.K.: Development of High Strength Al-Zn-Mg Alloys for Automotive Application, *Indian Foundry Journal*, Vol. 60, No. 4, April 2014, pp. 32-39.
12. Dupasquier, A., Ferragut, R., Iglesias, Macchi, C.E., Massazza, M., Mengucci, P., Riontino, G., Somoza, A., Early solute clustering in an AlZnMg alloy, *Materials Science Forum*, Vols. 445-446, 2004, pp. 16-20.
13. Clinch, M.R., Harris, S.J., Hepples, W., Holroyd, N.J.H., Lawday, M.J., Noble, B., Influence of Zinc to Magnesium Ratio and Total Solute Content on the Strength and Toughness of 7xxx series Alloys, *Materials Science Forum*, Vols. 519-521, 2006, pp. 339-344.
14. Costello, F.A., Robson, J.D., Prangnell, P.B.: The Effect of Small Scandium Additions to AA7050 on the As-cast and Homogeneous Microstructure, *Materials Science Forum*, Vols. 396-402, 2002, pp. 757-762.
15. Riddle, Y.W., Sanders, Jr., T.H.: Contribution of Al₃Sc to Recrystallization Resistance in Wrought Al-Sc Alloys, *Materials Science Forum*, Vols. 331-337, 2000, pp. 939-944.
16. Iwamura, S., Nakayama, M., Miura, Y.: Coherency between Al₃Sc Precipitate and the Matrix in Al Alloys Containing Sc, *Materials Science Forum*, Vols. 396-402, 2002, pp. 1151-1156.
17. Fuller, C.B., Krause, A.R., Dunand, D.C., Seidman, D.N.: Microstructure and mechanical properties of a 5754 aluminium alloy modified by Sc and Zr additions, *Materials Science and Engineering A338*, 2002, pp. 8-16.
18. Loffler, H., Kovacs, I., Lendvai, J., Review Decomposition processes in Al-Zn-Mg alloys, *Journal of Materials Science*, 18, 1983, pp. 2215-2240.
19. Ferragut, R., Somoza, A., Tolly, A., Torriani, I.: Precipitation kinetics in Al-Zn-Mg commercial alloys, *Journal of Materials Processing Technology*, 141, 2003, pp. 35-40.
20. Jiao, H., Li, C., The HREM Study of Precipitates in an Al-Zn-Mg Alloy, *Advanced Performance Materials*, 2, 1995, 305-309.
21. Salamci, E.: Calorimetric and transmission electron microscopy studies of spray deposited Al-Zn-Mg-Cu alloys, *Materials Science and Technology*, July 2004, Vol. 20, pp. 859-863.
22. X.M. Li, M.J. Starink, "DSC Study on Phase Transitions and Their Correlation with Properties of Overaged Al-Zn-Mg-Cu Alloys", *Journal of Materials Engineering and Performance*, Vol. 21(6), June 2012, pp. 977-984.
23. Zhenbo, H., Zhimin, Y., Sen, L., Ying, D., Baochuan, S., Xiang, Z.: Preparation, microstructure and properties of Al-Zn-Mg-Sc alloy tubes, *Journal of Rare Earths*, Vol. 28, No. 4, August 2010, pp. 641-646.
24. Santner, J.S.; Eylon, D.: Fatigue Behavior and Failure Mechanisms of Modified 7075 Aluminium Alloys, *Metallurgical Transactions A*, Vol. 10A, July 1979, pp. 841-848.

